



Biosynthesis of ZrO₂ nanoparticles from *Ficus benghalensis* leaf extract for photocatalytic activity

H. M. Shinde^{1,2} · T. T. Bhosale^{1,2} · N. L. Gavade¹ · S. B. Babar¹ · R. J. Kamble³ · B. S. Shirke² · K. M. Garadkar¹

Received: 14 March 2018 / Accepted: 21 June 2018 / Published online: 26 June 2018
© Springer Science+Business Media, LLC, part of Springer Nature 2018

Abstract

The biosynthesis of metal oxide nanoparticles (NPs) using plant extract is green, rapid, attractive and cost-effective approach. In the present study, we are reporting biosynthesis of ZrO₂ NPs as an efficient photocatalyst by using *Ficus benghalensis* (F.B.) leaf extract as a capping agent for the first time. To determine its optical, structural and morphological properties, the obtained ZrO₂ NPs were characterized by using UV–Vis, DRS, XRD, FT-IR, HR-TEM, FT-Raman and BET-surface area. XRD pattern confirms that biosynthesized ZrO₂ NPs are crystalline in nature with monoclinic and tetragonal structure. TEM images show that the obtained ZrO₂ NPs has spherical morphology with 15 nm in size which is good agreement with XRD results. A decrease in the band gap of bulk ZrO₂ from 5.3 to 4.9 eV is observed due to the quantum size effect. The as-synthesized ZrO₂ NPs have high specific surface area of 88 m²/g was obtained by BET analysis. The photocatalytic efficiency of ZrO₂ NPs is evaluated for the photodegradation of methylene blue and methyl orange dyes as the target pollutants under UV light irradiation. The different parameters like catalyst loading amount and pH have also been studied. It is observed that photodegradation of methylene blue and methyl orange up to 91 and 69% within 240 min by using ZrO₂ catalyst. Moreover, this green synthesis process provides a valuable alternative to orthodox multistep processes for the preparation of ZrO₂ NPs.

1 Introduction

In the era of nanotechnology, the demand of nanosize materials increases day by day which is used to describe the creation and utilization of materials with structural features between those of atoms and bulk materials [1, 2]. ZrO₂ is widely used in various fields such as dental, energy, gas sensors, fuel cells, refractory materials due to its admirable properties [3–5]. ZrO₂ nanomaterial has attracted major research interest due to its unique optical, electrical, mechanical and biocompatible properties,

it is a kind of p-type semiconductor which shows both oxidizing and reducing ability due to its acidic and basic nature [6, 7]. The wide band gap and the high negative value of conduction band potential of ZrO₂ easily produces oxygen holes as a carrier of catalyst, hence generates interaction with active components [8–10]. The high band gap energy and high stability of ZrO₂ nanoparticles (NPs) make it good photocatalyst [11]. ZrO₂ NPs have three crystal phases, that is, cubic (c-ZrO₂), tetragonal (t-ZrO₂), and monoclinic (m-ZrO₂), under normal atmosphere and different temperatures [12]. The m-ZrO₂ phase is thermodynamically stable up to 1100 °C, t-ZrO₂ phase exists in the temperature range of 1100–2370 °C, and the cubic phase is found to stable above 2370 °C [13]. ZrO₂ NPs were fabricated widely using several chemical and physical methods such as hydrothermal, electrochemical, laser ablation, microwave irradiation, and photochemical because of its high growth rate [14, 15]. However, due to negative impacts of chemical methods on the environment and to fulfill the growing needs of environmental friendly NPs, it is an urgent need to replace chemical preparation methodology with clean, non-toxic and environmentally friendly, green chemistry approaches [16]. Nowadays, plant extract has been used as reducing and capping agent

✉ B. S. Shirke
bss_chemistry@yahoo.com

✉ K. M. Garadkar
kmg_chem@unishivaji.ac.in

¹ Nanomaterials Research Laboratory, Department of Chemistry, Shivaji University, Kolhapur, Maharashtra 416004, India

² Material Science Laboratory, Department of Chemistry, Y.C. Warana Mahavidyalaya, Warananagar, Maharashtra 416113, India

³ Department of Physics, Jaysingpur College, Jaysingpur, Maharashtra 416101, India

for the synthesis of NPs which could be advantageous over microbial synthesis because there is no need of the elaborated process of culturing, maintaining and recoiling the cell culture [17]. Recently plant leaf extract of *Nyctanthes arbor-tristis* [18], *Acalypha indica* [19], *Azadirachta indica* [20], *Capsicum annuum*, *Allium cepa*, *Lycopersicon esculentum* [21] have been used for the synthesis of ZrO_2 NPs. The synthesis of metal NPs using plant extract is a combination of green chemistry and nanotechnology, which eliminate hazardous chemicals for the synthesis of metal NPs by reduction and also, the shape and size can be controlled without toxic and harsh chemicals. In this study we have biosynthesized ZrO_2 NPs by using *Ficus benghalensis* (Banyan tree) leaf extract for the first time. There are more than 800 species and around 2000 varieties of F.B., which is a national tree of India. F.B. leaves contain crude protein 9.63%, crude fibres 26.84%, CaO 2.53% and Phosphorus 0.4% [22–24]. The biosynthesized ZrO_2 NPs were characterized by diffuse reflectance spectroscopy (DRS), transmission electron microscopy (TEM), X-ray diffraction (XRD), and scanning electron microscopy with energy dispersive X-ray (SEM-EDS). The biogenic ZrO_2 NPs were used for the photocatalytic degradation of the methylene blue (MB) and methyl orange (MO) dye.

2 Experimental details

2.1 Material and method

Fresh leaves of F.B. (*banyan tree*) were procured locally from Shivaji University Campus, Kolhapur (India). $ZrOCl_2 \cdot 8H_2O$ was purchased from Spectrochem Pvt. Ltd., Mumbai (India). Methylene blue and methyl orange were purchased from Spectrochem Pvt. Ltd., Mumbai (India). All the chemicals were of analytical grade and used without further purification. Deionized water was used throughout the experiment. All glassware used for the preparation of ZrO_2 NPs was properly washed with a soap solution followed by distilled water and dried in a hot air oven.

2.2 Preparation of plant extract

The procured fresh leaves of F.B. were washed initially with running tap water for several times followed by deionized water to remove debris, other contamination and shade dried to remove residual moisture. Then 5 g of dried leaves were finely crushed and boiled in 100 mL of deionized water for 15 min until color changes to pale brown. After that leaf

extract was filtered through Whatman filter paper No. 1. The filtrate was kept in a refrigerator for further work.

2.3 Biosynthesis of ZrO_2 NPs

For biosynthesis of ZrO_2 NPs, 20 mL of leaf extract was added dropwise into 20 mL of (0.1 M) aqueous $ZrOCl_2 \cdot 8H_2O$ solution with constant stirring using magnetic stirrer. The resultant solution was evaporated up to dryness in a microwave oven at 900 W for 15 min (20 s on–40 s off cycle). The product obtained was grounded for 15 min. using mortar pestle to form a fine powder. Then this powder was calcinated at 500 °C for 3 h. in a temperature controlled muffle furnace. A schematic representation of biosynthesis of ZrO_2 NPs is shown in Fig. 1.

2.4 Characterization of ZrO_2 NPs

The morphology and particle size of synthesized ZrO_2 NPs sample were investigated by a TEM (JEOL JEM 2100). The elemental composition of synthesized ZrO_2 NPs obtained by EDS attached to SEM (Carl-Zeiss), Model LEO 1430 VP, Germany. Surface area and total pore volume were obtained by using BET-surface area (Quantachrome NOVA1000e, USA). The XRD pattern of ZrO_2 NPs was recorded by using Panalytical Diffractometer with $CuK\alpha$ radiation. FT-Raman spectrum was obtained using an FT-Raman (BRUKER RFS 27) to determine different phases of ZrO_2 NPs. FT-IR spectra were obtained using an FT-IR (FT/IR-4600 type A D044761786). Diffuse reflectance spectrum (DRS) of ZrO_2 NPs was obtained by using UV–Vis Spectrophotometer (JASCO V-770).

2.5 Photocatalytic activity

The photocatalytic activity of ZrO_2 NPs was evaluated by monitoring the degradation of MB and MO dyes under UV light (365 nm). High-pressure mercury lamp (Philips

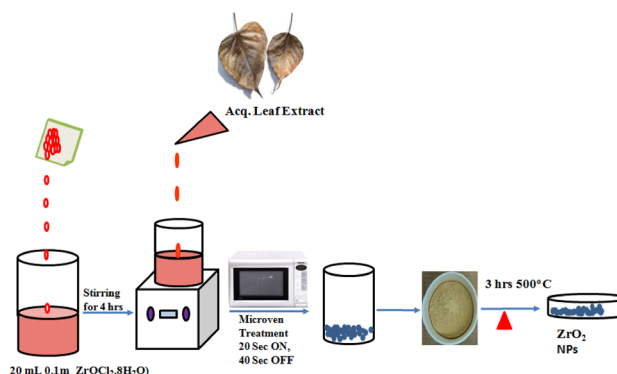


Fig. 1 Schematic representation of biosynthesis of ZrO_2 NPs

HPL-N, 250 W) was used as a UV source. The degradation experiments were performed at room temperature in a photochemical reactor. To estimate the best photocatalytic activity, the quantity of photocatalyst was varied from 0.5 to 2.0 g/dm³ in a dye solution. The effect of pH on the photocatalytic activity was also studied by varying pH of the solution from 3 to 9 using HCl and NaOH (1 M) each. Typically, in this photodegradation experiments the optimum quantity (1.5 g/dm³) of photocatalyst was added in a photoreactor containing 100 mL of dye solution. Before irradiation of light, the dye solution was stirred for 30 min. in dark to ensure adsorption–desorption equilibrium, then exposed to UV light. During the course of irradiation sufficient amount of aliquots were collected at a fixed time interval and centrifuged to separate the photocatalyst. Then, the absorbance of the supernatant was measured by using a UV–Vis Spectrophotometer (Shimadzu Model—UV-3600).

The percentage degradation of dyes were calculated by using the following formula,

$$\text{Degradation (\%)} = \frac{C_0 - C_t}{C_0} \times 100 \quad (1)$$

where C_0 and C_t represent the initial concentration and concentration after time (t) of MB respectively.

3 Results and discussion

3.1 XRD analysis of ZrO₂ NPs

The formation of biosynthesized ZrO₂ NPs confirmed by XRD as shown in Fig. 2. The prominent diffraction peaks located at $2\theta = 28.34^\circ$, 30.23° , 35.17° , 40.44° , 50.30° , 60.18° , 62.75° and 75.05° were indexed to the (111), (111), (200), (102), (220), (311), (222) and (400),

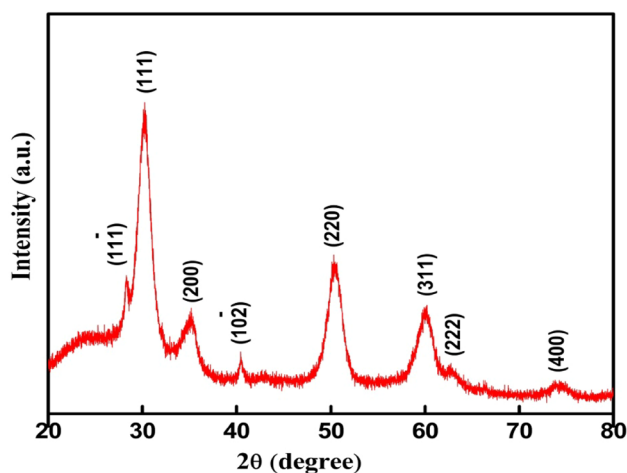


Fig. 2 XRD pattern of ZrO₂ NPs

(200), (102), (220), (311), (222) and (400) diffraction planes respectively, which is well agreed to JCPDS (Card No. 37-1484 and 42-1164) [25]. This indicates the synthesized ZrO₂ NPs consist of both monoclinic and tetragonal phases. The average crystallite size of ZrO₂ NPs was found to be 7 nm, calculated by using Scherrer's equation,

$$D = \frac{0.9\lambda}{\beta \cos \theta} \quad (2)$$

where λ is the wavelength of the target CuK α radiation (1.5406 Å), θ is Bragg's diffraction angle, and β is full width at half maximum (FWHM) in radian.

3.2 FT-Raman analysis of ZrO₂ NPs

Raman scattering is an effective technique to investigate the crystallization, structure and defects in the group theory. Figure 3 shows the FT-Raman spectrum of powder sample of ZrO₂ calcined at 500 °C. The Raman spectrum indicates bands at 150.59, 271.87, 319.03, 519.59 and 562.41 cm⁻¹ that are characteristic bands of tetragonal ZrO₂ and FT-Raman bands at 86.62 and 191.91 cm⁻¹ are exclusively assigned to the monoclinic phase. The band at 466.45 and 639.70 cm⁻¹ are common for both phases but relatively intensity is different [26, 27].

3.3 FT-IR analysis of ZrO₂ NPs

FT-IR analysis was performed to determine functional groups present in F.B. leaf extract and biosynthesized ZrO₂ NPs displayed in Fig. 4. The FT-IR spectrum of aqueous leaf extract of F.B. indicates major absorption peaks at 3314, 1629, 1531, 1495 and 1184 cm⁻¹ respectively as shown in Fig. 4a. The peak at 1629 cm⁻¹ belongs to C–H stretching

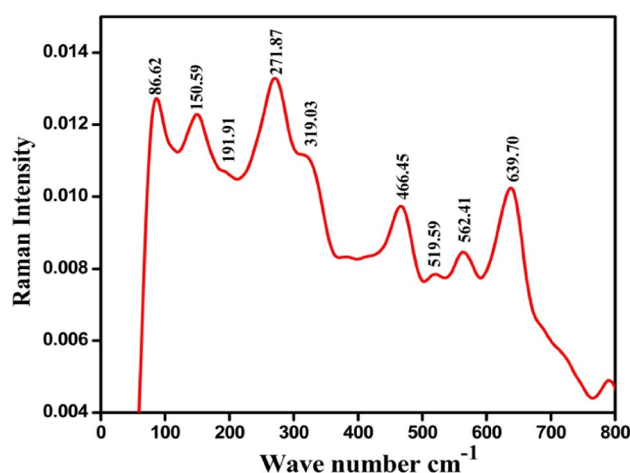


Fig. 3 FT-Raman spectra of ZrO₂ NPs

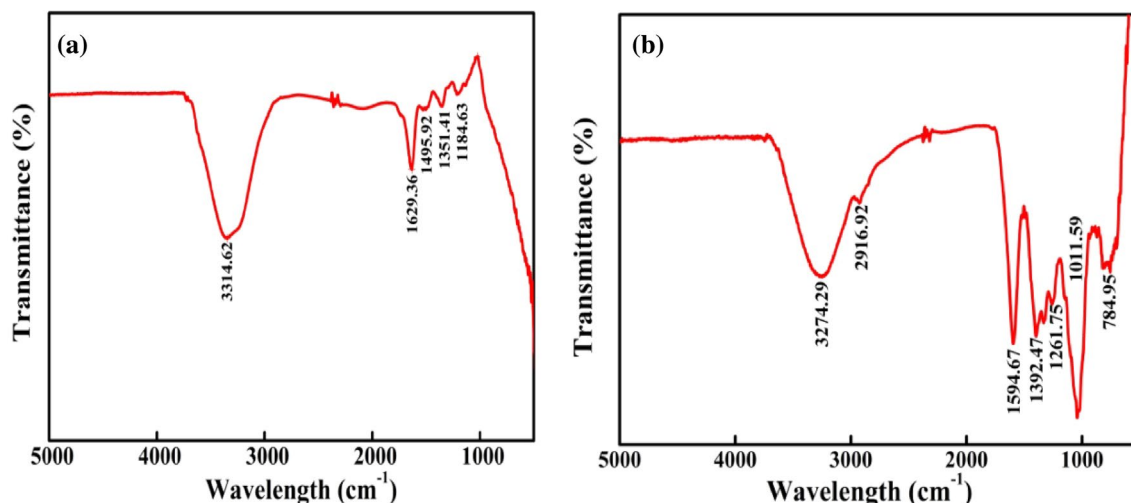


Fig. 4 **a** FT-IR Spectrum of *Ficus benghalensis* leaf extract and **b** ZrO_2 NPs

vibration. The pattern of absorption in the region around 1531 and 1495 cm^{-1} belongs to C=O of stretching vibration [28, 29]. Figure 4b shows the FT-IR spectrum of biosynthesized ZrO_2 . The broad prominent peak located at 3274 cm^{-1} corresponds to O–H stretching vibration owing to moisture absorbed on the sample surface. The peak located around 1594 cm^{-1} related to vibration accruing due to C=O stretching. The absorption peak between 784 and 1011 cm^{-1} region is characteristics of Zr–O–Zr vibrations, which confirms the formation of crystalline ZrO_2 NPs [30, 31]. That indicates the formation of ZrO_2 NPs possible involvements of carboxyl groups, amines, intermediate form of phenolic groups, proteins and carbohydrates of F.B. leaf extract in the reduction processes for the synthesis of ZrO_2 NPs.

3.4 UV–Vis diffuse reflectance spectra of ZrO_2 NPs

The UV–Vis diffuse reflectance spectrum of ZrO_2 NPs is shown in Fig. 5a. DRS spectrum of the samples exhibited strong absorption in the UV region around 240–350 nm due to the charge transition from oxide species to zirconium cation ($O^- \rightarrow Zr^{4+}$) [32]. The band gap energy is important for the photocatalytic activity because the energy of incident light must be greater than or equal to the band gap energy is the criteria to select the photocatalyst. Therefore, the optical band gap with direct transition can be calculated from the following equation.

$$(\alpha h\nu) = A(h\nu - E_g)^{1/2} \quad (3)$$

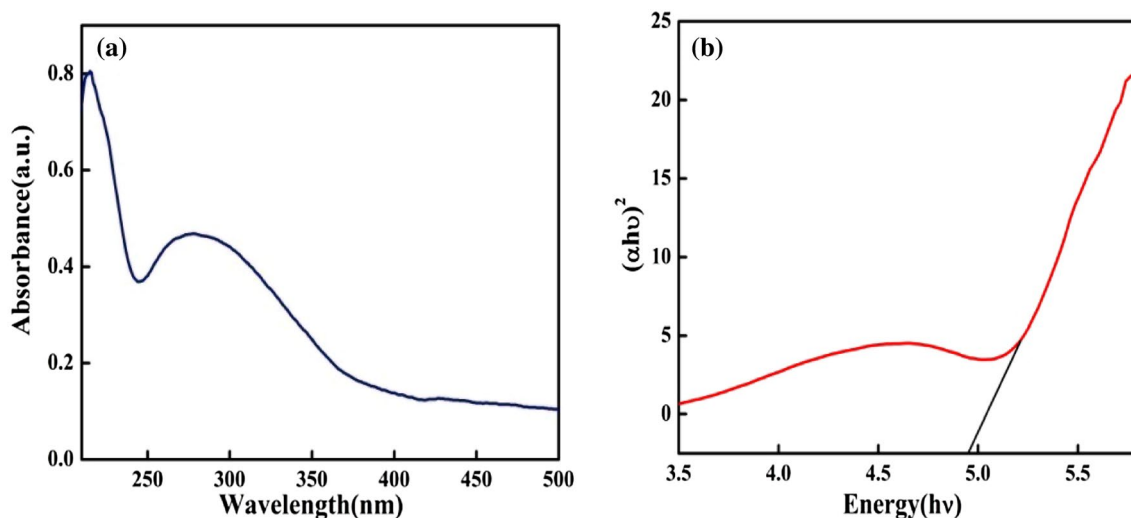


Fig. 5 **a** DRS spectrum of ZrO_2 and **b** Tauc plot of ZrO_2

where α , h , A , and E_g are the absorption coefficient, frequency, proportionality constant and band gap energy respectively. The accurate band gap of ZrO_2 found to be 4.9 eV, which was obtained by plotting of $(\alpha h\nu)^2$ versus photon energy ($h\nu$) as shown in Fig. 5b. The observed band gap value is similar to the value reported in the literature [33].

3.5 EDS analysis and color mapping

EDS spectrum of biosynthesized ZrO_2 NPs was used to investigate the elements presents in the sample as shown in Fig. 6a. The spectrum consists of intense peaks of Zr at 2.2 eV and of O at 0.5 eV. The presence of intense peaks of Zr and O in EDS spectra clearly indicates the formation and composition of crystalline ZrO_2 NPs. No other peaks were observed from EDS that confirm the high purity of the sample. The quantitative analysis of EDS revealed the atomic % of Zr and O are 21.13 and 78.13% respectively. Figure 6b shows the color mapping of ZrO_2 NPs.

3.6 TEM images of ZrO_2 NPs

TEM analysis was carried out to get information about the size and morphology of the ZrO_2 . Figure 7a, b shows TEM images of ZrO_2 NPs with various magnifications. From the TEM images, it is seen that particle size of ZrO_2 NPs are in the range of 10–18 nm and spherical in shape. The interplanar spacing (d) value 0.28 nm is observed from the HR-TEM as shown in Fig. 7c. The selected area electron diffraction pattern (SAED) of ZrO_2 NPs shown in Fig. 7d, SAED pattern indicates that the particles are nanocrystalline in nature. The interplanar spacing (d) values obtained from HR-TEM matches with the XRD results, which proves the ZrO_2 NPs are monoclinic and tetragonal in structure.

In order to estimate the average particle size of ZrO_2 NPs, histograms was drawn as shown in Fig. 8.

3.7 BET analysis of ZrO_2 NPs

Photocatalytic activity highly depends on the surface area of the photocatalyst, as surface area increases photocatalytic activity also increases. BET analysis gives the surface area and total pore volume of the biosynthesized ZrO_2 NPs are about 88 m^2/g and 1.36 cc/g respectively, such high surface area is responsible for enhancing the photocatalytic degradation of dye [34]. The nitrogen adsorption–desorption shows a hysteresis loop that is extremely equivalent to type V isotherm as shown in Fig. 9. The average particle size was estimated by assuming all the particles to have same spherical shape. The relation between the specific surface area and the particle size of BET model is

$$d = \frac{6000}{(S_{BET} \times \rho)} \quad (4)$$

where S_{BET} is a surface area, ρ is solid density (for ZrO_2 is 5.68 g/mL) and d is particle size. The average particle size of ZrO_2 NPs was calculated by this model is 15 nm, which is good agreement with TEM results [35].

3.8 Plausible mechanism for the synthesis of ZrO_2 NPs

The polyphenols present in the aqueous leaf extract bind the surface of zirconium in zirconium chloride to activate the complex formation with the bridge-like network between $-OH$ groups. The $-OH$ groups from the polyphenols act as a capping agent and also controls the size of ZrO_2 NPs. The formation mechanism of the ZrO_2 NPs is shown in Fig. 10.

Fig. 6 a EDS spectrum and b color mapping of ZrO_2 NPs

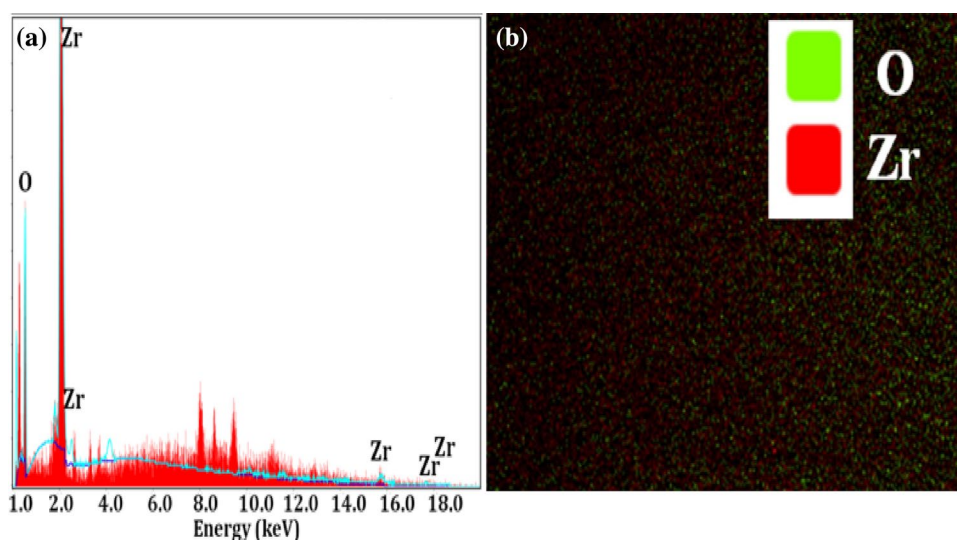


Fig. 7 **a, b** TEM images with different magnifications, **c** HR-TEM and **d** SAED pattern of ZrO_2 NPs

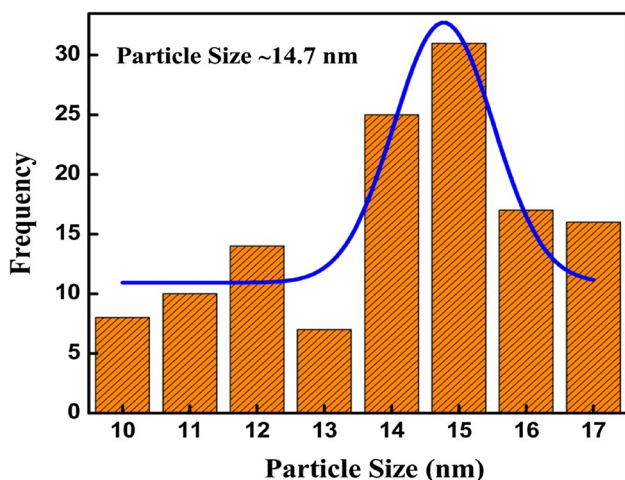
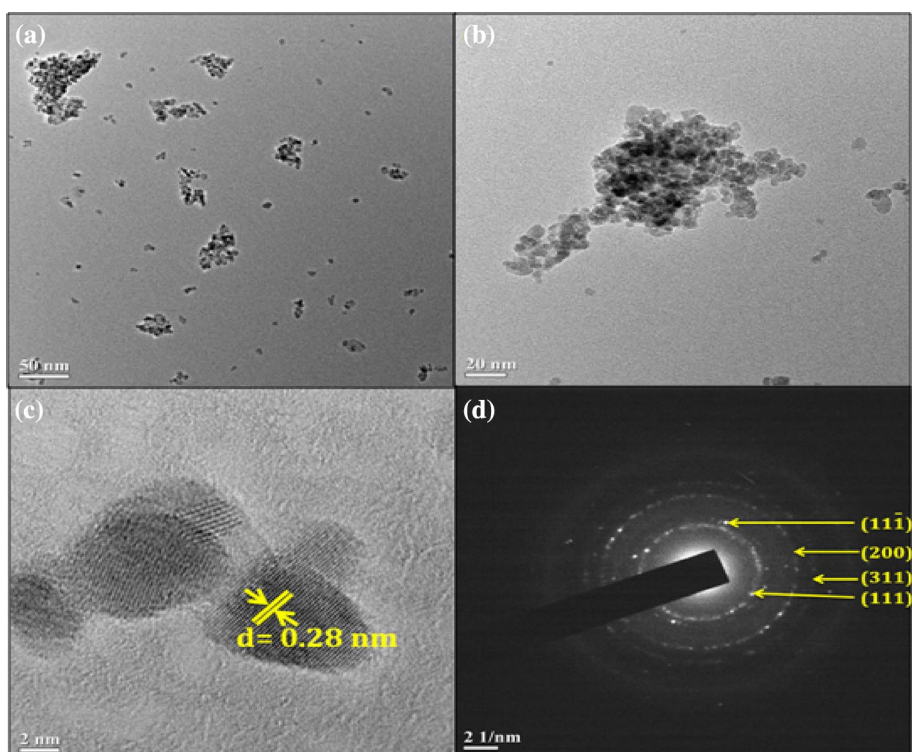


Fig. 8 Histogram of ZrO_2 NPs with size distribution

3.9 Photocatalytic activity of ZrO_2 NPs

The photocatalytic degradation of MB and MO dyes under UV light with and without using ZrO_2 photocatalyst was investigated. To know the photolysis we tested the photodegradation of dyes without adding catalyst (in absence of ZrO_2) under UV light and we observed 7.36 and 3.73% degradation efficiency of MB and MO dyes respectively within 240 min. In the presence of ZrO_2 catalyst the degradation efficiency

of MB (5 ppm) and MO (20 ppm) was found to be 91.22 and 69.23% respectively as shown in Fig. 11a, b. The comparisons of photodegradation efficiency of biosynthesized ZrO_2 with previously reported ZrO_2 photocatalyst synthesized by various methods for degradation of MB and MO dyes are summarized in Table 1, that indicates the ZrO_2 NPs synthesized by biogenic method, exhibited better degradation efficiency (91%) and (69%) for the photodegradation of MB and MO dyes under UV light irradiation within 240 min [36–38].

3.9.1 Effect of catalyst loading

For a commercial point of view, it is essential to find out the optimum amount of catalyst, to avoid the excess use. To examine the effect of catalyst loading on the rate of degradation efficiency of MB (5 ppm) and MO (20 ppm) was studied under UV light. Hence, amount of catalyst varied from 0.5 to 2.0 g/dm^3 by keeping other parameters identical. The result of this study is shown in Fig. 12. It is observed that degradation efficiency of both MB and MO dyes initially increases from 38 to 56 and 17 to 29% with an increase in the amount of catalyst from 0.5 to 1.5 g/dm^3 within 60 min. The degradation efficiency of MB and MO dyes were observed higher with 1.5 g/dm^3 catalyst and then the further rate of degradation efficiency of MB and MO dyes decreases from 56 to 43 and 29 to 19% as the catalyst amount increased from 1.5 to 2.0 g/dm^3 . Photocatalysis reaction depends upon the concentration of reactant and active sites of the photocatalyst

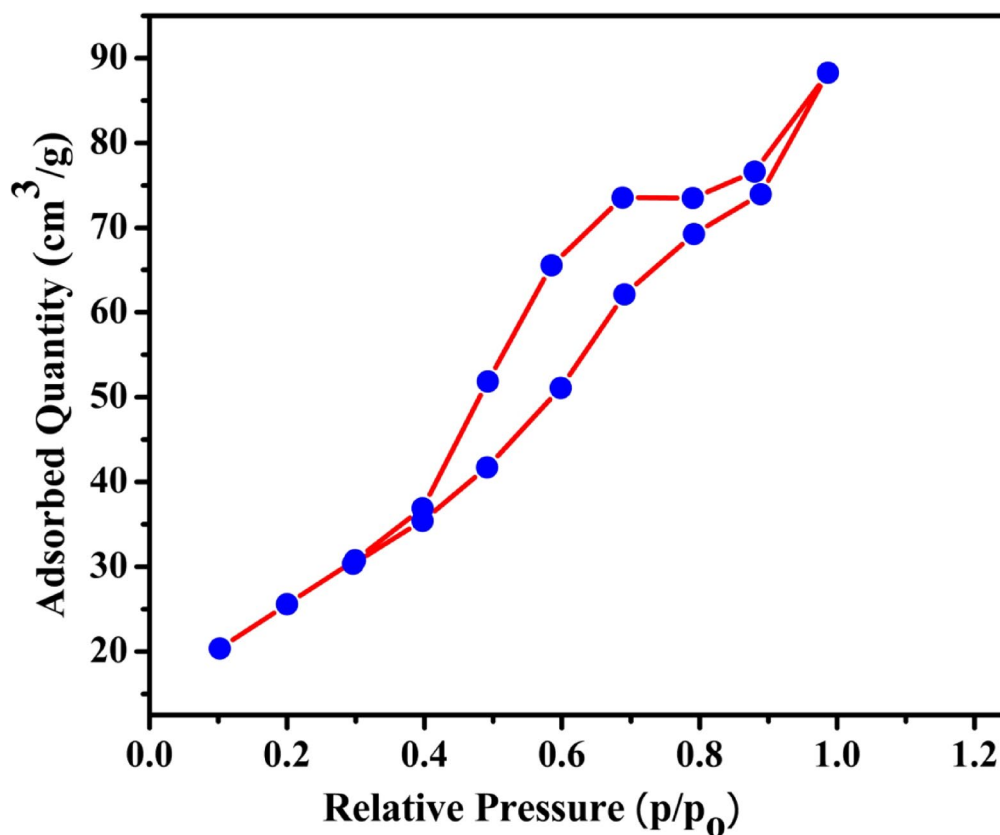


Fig. 9 N_2 -adsorption–desorption curves

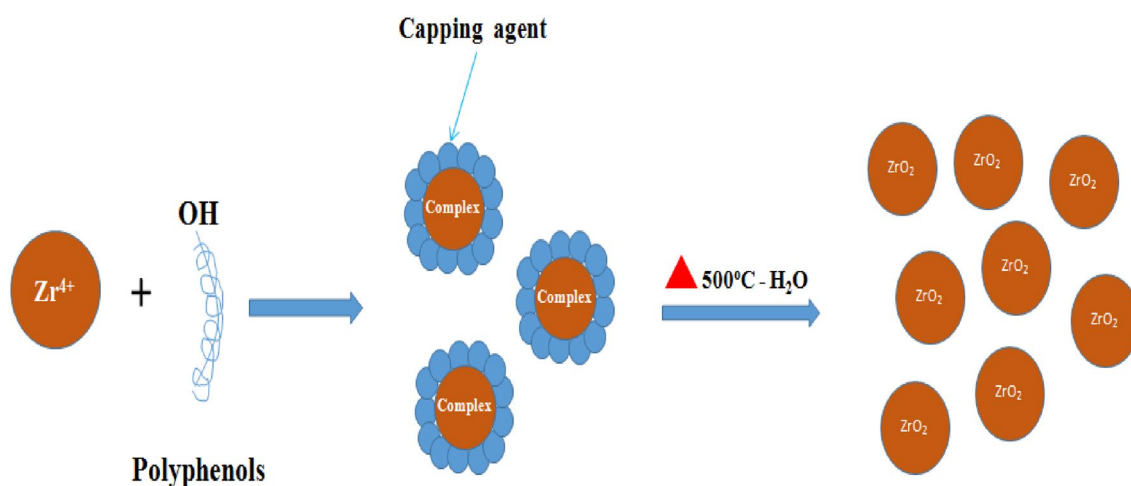


Fig. 10 Plausible mechanism for the formation mechanism of ZrO_2 NPs

surface. We observed that with increasing amount of catalyst the rate of photocatalytic degradation reaction also improves due to increasing the number of active sites on the photocatalyst [39]. However, above 1.5 g/dm^3 the rate of photocatalytic degradation reaction decreased, due to agglomeration of the catalyst which results to decrease in the number

of active sites on the photocatalyst. Another factor for the decrease in photocatalysis efficiency at high catalyst loading is the turbidity of suspension, which is attributed to the inhibition of photon absorption on the catalytic surface of the catalyst, because of scattering light dominates at higher catalyst loading [40, 41].

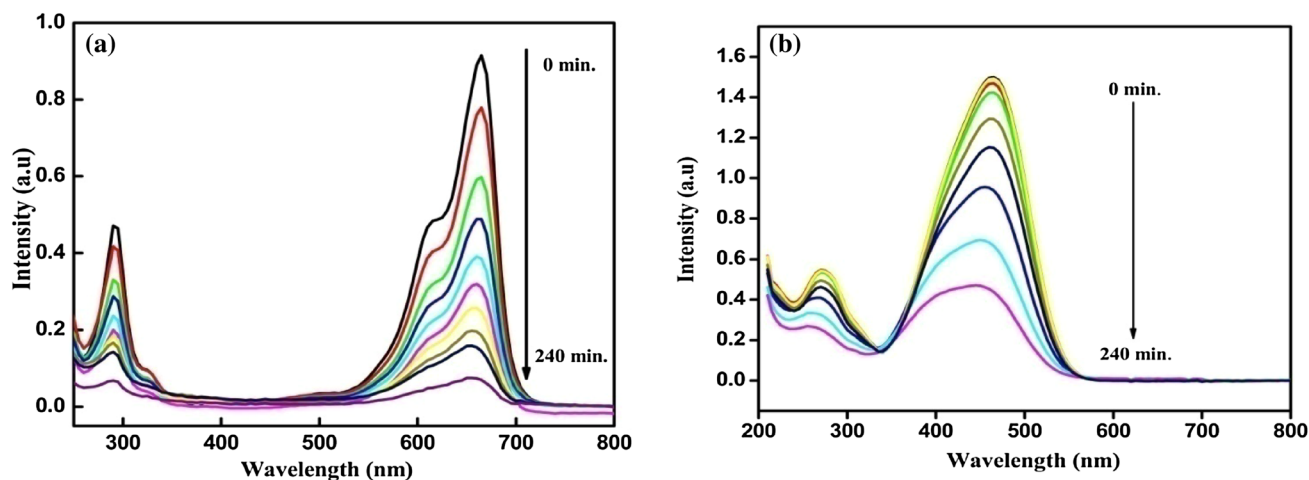


Fig. 11 a UV absorption spectra of MB at different time. b UV absorption spectra of MO at different time

Table 1 Comparison of the catalytic performance of ZrO_2 with some of the previously various reported synthetic methods for degradations of MB and MO dyes

Photocatalyst	Synthetic method	Dye	Degradation time	Degradation efficiency %	References
1. FS-ZrNTs	Anodisation	MO	300 min	70	[36]
2. N- ZrO_2	Thermal decomposition	MB	240 min	59	[37]
3. ZrO_2	Polymer-assisted	MB	24 h	68	[38]
4. ZrO_2	Biogenic	MB	240 min	91	Present work
		MO		69	

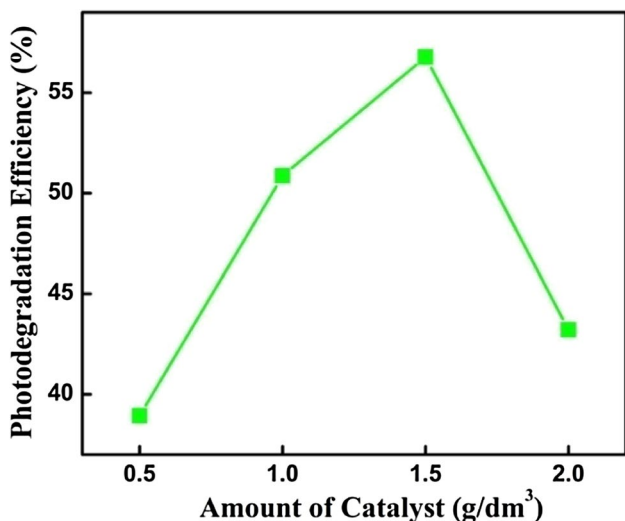


Fig. 12 Effect of catalyst loading on the degradation of MB

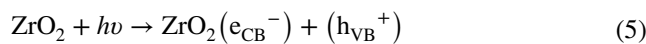
3.9.2 Effect of pH

pH is an important parameter for the photocatalytic degradation of wastewater because industrial effluent may be complex in nature. This can affect the photocatalytic degradation efficiency of MB and MO dyes, therefore the effect

of pH need to be investigate. To study the effect of pH of the dye solution on the degradation efficiency, the photocatalytic degradation experiment were carried out at different values of pH of MB and MO ranging from 3 to 9 at optimal catalyst loading (1.5 g/dm^3), suspension with pH less than 3 were not considered due to the dissolution of ZrO_2 as shown in Fig. 13. It is observed that there was no significant change in photocatalytic activity at pH 3, 5 and 9 almost showed similar degradation efficiency of both MB and MO. The effect of pH depends on the point of zero charges of the catalyst. If the pH of the solution is lower than the point of zero charges, the ZrO_2 surface will be positively charged, which is favorable for the adsorption. The maximum photodegradation 91.22 and 69.23% of MB and MO dyes was observed at pH 7, which is below the zero point charge of the ZrO_2 catalyst [42, 43].

3.9.3 Mechanism of photodegradation

The mechanism of photocatalytic degradation involves adsorption of the MB and MO dye on the surface of ZrO_2 catalyst, when exposed to UV light irradiation can be illustrated as follows.



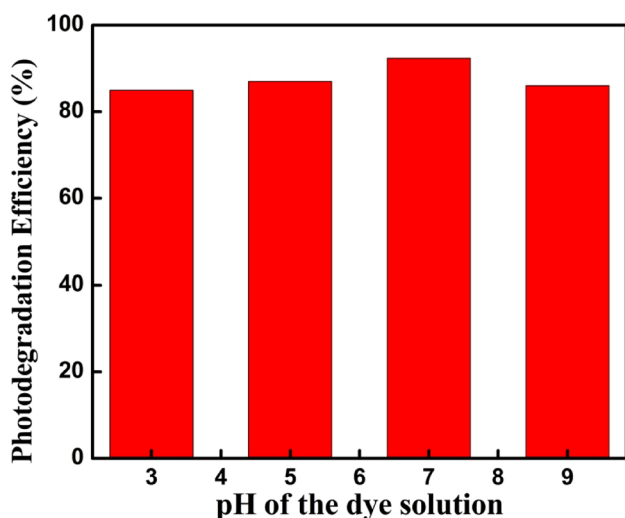
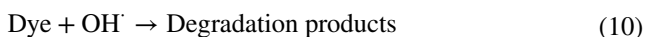
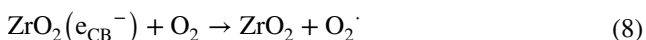
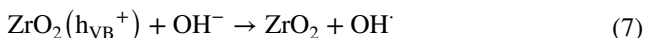
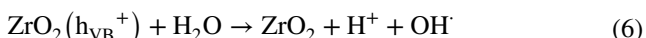


Fig. 13 Effect of initial pH of MB on photodegradation



It leads to the generation of electrons (e^-) in the conduction band of ZrO_2 , which interact with the oxygen molecules adsorbed on ZrO_2 to produce superoxide anion radicals ($\text{O}_2^- \cdot$). The holes generated in the valence band of ZrO_2 acts as an oxidizing agent and react with surface hydroxyl groups to form highly reactive hydroxyl radicals (OH^-). The highly reactive hydroxyl radicals (OH^-) reacts with a dye adsorbed on ZrO_2 catalyst and lead to its degradation [44, 45]. The schematic representation of degradation process of dye by using ZrO_2 NPs is shown in Fig. 14.

4 Conclusions

A biosynthesis of ZrO_2 NPs was achieved using *Ficus benghalensis* leaf extract for efficient photocatalysis. The monoclinic and tetragonal structure of the synthesized ZrO_2 NPs are confirmed by XRD pattern. TEM analysis shows that average particle size of ZrO_2 NPs are 15 nm. The FT-IR results show the possible involvement of groups in biochemical reactions are protein, polyphenols, terpenoids, amines, and carboxylic acids. The FT-Raman analysis shows the ZrO_2 consist of both monoclinic and

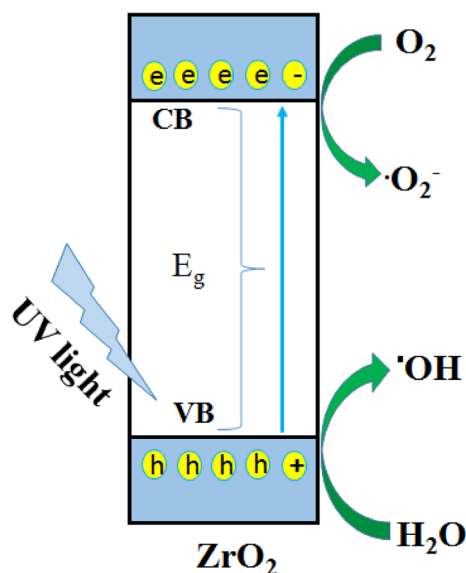


Fig. 14 Schematic model for the mechanism of photodegradation

tetragonal phases. The DRS spectrum confirms that the synthesized ZrO_2 has high absorbance with 4.9 eV band gap. Biosynthesized ZrO_2 NPs consist high surface area about $88 \text{ m}^2/\text{g}$. The efficiency for the removal of MB and MO is about 91 and 69%. Biosynthesized ZrO_2 shows good photocatalytic activity than the ZrO_2 synthesized by other methods.

Acknowledgements Authors are thankful to SAIF-NEHU, Shillong for providing TEM Facility. Authors are also thankful to DST-FIST (No/SR/FST/College-151/2013(C)) for providing Instrumentation Facility.

References

1. A. Saxena, R.M. Tripathi, F. Zafar, P. Singh, Mater. Lett. **67**, 91 (2012)
2. A. Bhirud, S. Sathaye, R. Waichal, C.J. Park, B. Kale, J. Mater. Chem. A. **3**, 17050 (2015)
3. W. Cao, J. Kang, G. Fan, L. Yang, F. Li, Ind. Eng. Chem. Res. **54**, 12795 (2015)
4. B.H. Cho, W.B. Ko, J. Nanosci. Nanotechnol. **13**, 7625 (2013)
5. H. Zhang, H. Lu, Y. Zhu, F. Li, R. Duan, M. Zhang, X. Wang, Powder Technol. **227**, 9 (2012)
6. K. Gurushantha, K.S. Anantharaju, L. Renuka, S.C. Sharma, H.P. Nagaswarupa, S. Prashantha, Y.S. Vidya, H. Nagabhushana, RSC Adv. **7**, 12690 (2017)
7. L. Zhu, G. He, Z.Q. Sun, M. Liu, S.S. Jiang, S. Liang, W.D. Li, J. Sol-Gel. Sci. Technol. **83**, 675 (2017)
8. J. Li, S. Meng, J. Niu, H. Lu, J. Adv. Ceram. **6**, 43 (2017)
9. S.N. Basahel, T.T. Ali, M. Mokhtar, K. Narasimharao, Nanoscale Res. Lett. **10**, 73 (2015)
10. S. Ambika, M. Sundrarajan, J. Photochem. Photobiol. B **146**, 52 (2015)
11. N.L. Gavade, A.N. Kadam, Y.B. Gaikwad, M.J. Dhanavade, K.M. Garadkar, J. Mater. Sci. Mater. Electron. **27**, 11080 (2016)

12. A. Majedi, A. Abbasi, F. Davar, *J. Sol-Gel. Sci. Technol.* **77**, 542 (2016)
13. T. Chraska, A.H. King, C.C. Berndt, *Mater. Sci. Eng.* **286**, 169 (2000)
14. J.H. Lee, S.J. Park, *J. Am. Ceram. Mater.* **17**, 3997 (2005)
15. W. Liang, T.L. Church, A.T. Harris, *Green Chem.* **14**, 968 (2012)
16. N.L. Gavade, S.B. Babar, A.N. Kadam, A.D. Gophane, K.M. Garadkar, *Ind. Eng. Chem. Res.* **56**, 14489 (2017)
17. L.P. Bauermann, J. Bill, F. Aldinger, *J. Phys. Chem. B* **110**, 5182 (2006)
18. S. Li, Y. Shen, A. Xie, X. Yu, L. Qiu, L. Zhang, Q. Zhang, *Green Chem.* **14**, 852 (2007)
19. S. Shanthi, S. Tharani, *Int. J. Eng. Appl. Sci.* **3**, 23 (2016)
20. P. Nimare, A.A. Koser, *Int. Res. Eng. Technol.* **3**, 1910 (2016)
21. R.A. Jalill, M.M. Jawad, N.A. Abd, *J. Genet. Environ. Resour. Conserv.* **5**, 6 (2017)
22. R.M. Tripathia, A. Shrivastava, B.R. Shrivastav, *Int. J. Pharma Bio Sci.* **3**, 551 (2012)
23. K. Roy, H. Shivakumar, S. Sarkar, *Int. J. PharmTech Res.* **1**, 3 (2009)
24. M. Govindarajan, *Eur. Rev. Med. Pharmacol. Sci.* **14**, 107 (2010)
25. A. Akbar, A.A. Ashkarran, S.A.A. Afsar, S.M. Aghigh, M. Kavianipour, *Polyhedron* **29**, 1370 (2010)
26. F. Davar, M.R. L-Estarki, *Ceram. Int.* **40**, 8427 (2014)
27. F. Davar, A. Hassankhani, M.R. L-Estarki, *Ceram. Int.* **39**, 2933 (2013)
28. K. Saware, B. Sawle, B. Salimath, K. Jayanthi, V. Abbaraju, *Int. J. Res. Eng. Technol.* **3**, 867 (2014)
29. R. Papitha, L. Ravi, R. Kaviyarasi, M. Bhuvanewari, *Int. J. Green Pharm.* **11**, 127 (2017)
30. S. Poliseti, P.A. Deshpande, G. Madras, *Ind. Eng. Chem. Res.* **50**, 12915 (2011)
31. T. Hirata, E. Asari, M. Kitajima, *J. Solid State Chem.* **110**, 201 (1994)
32. V. Emeline, G.N. Kuzmin, D. Purevdorj, V.K. Ryabchuk, N. Serpone, *J. Phys. Chem. B* **104**, 2989 (2000)
33. L. Xie, J. Wang, Y. Hu, S. Zhu, Z. Zheng, S. Weng, P. Liu, *RSC Adv.* **2**, 988 (2012)
34. K.J.A. Raj, B. Viahwanathan, *Indian J. Chem. A* **48A**, 1378 (2009)
35. I. A. Opalinska, W. Malka, T. Dzwolak, A. Chudoba, W. Presz, Lojowski, *J. Nanotechnol.* **6**, 627 (2015)
36. M. Rozana, N.I. Soaid, T.W. Kian, G. Kawamura, A. Matsuda, Z. Lockman, *J. Nanotechnol.* **28**, 1 (2017)
37. H. Sudrajat, S. Babel, H. Sakai, S. Takizawa, *J. Environ. Manag.* **165**, 224 (2016)
38. C. Dhandapani, R. Narayanasamy, S.N. Karthick, K.V. Hemalatha, S. Selvam, P. Hemalatha, M.S. Kumar, S.D. Kirupha, H.M. Kim, *Optik* **127**, 10288 (2016)
39. V.V. Gawade, N.L. Gavade, H.M. Shinde, S.B. Babar, A.N. Kadam, K.M. Garadkar, *J. Mater. Sci. Mater. Electron.* **28**, 14033 (2017)
40. S.B. Gajbhiye, *Int. J. Mod. Eng. Res.* **2**, 1204 (2012)
41. M.B. Suwarnkar, R.S. Dhabbe, A.N. Kadam, K.M. Garadkar, *J. Ceram. Int.* **40**, 5489 (2014)
42. P. Jantawasua, T. Sreethawonga, S. Chavadej, *Chem. Eng. J.* **155**, 223 (2009)
43. I. Kazeminezhad, A. Sadollahkhani, *J. Mater. Sci. Mater. Electron.* **27**, 4206 (2017)
44. Z.M. Abou-Gamra, M.A. Ahmed, *J. Photochem. Photobiol. B* **160**, 134 (2016)
45. M.A. Tayeb, D.S. Hussein, *Am. J. Nanomater.* **3**, 57 (2015)